Gas Diffusion and Microstructural Properties of Ordered Mesoporous Silica Fibers

Hatem M. Alsyouri[†,‡] and Jerry Y. S. Lin*[,†,§]

Department of Chemical Engineering, University of Cincinnati, Cincinnati, Ohio 45221, and Department of Chemical and Material Engineering, Arizona State University, Tempe, Arizona 85287-6006

Received: February 24, 2005; In Final Form: May 16, 2005

Pore and surface diffusion of carbon dioxide (CO_2) and ethylene (C_2H_4) in the nanopores of ordered mesoporous silica fibers about 200 μm in length was measured by the transient gravimetric method. The experimentally determined pore diffusivity data, coupled with the porosity, pore size, and fiber length, are used to obtain the actual length of the nanopores in silica fibers. These measurements reveal a structure of the ordered nanopores whirling helically around the fiber axis with a spiral diameter of about 15 μm and a pitch value of 1.6 μm. At room temperature the surface diffusion contributes about 10% to the total diffusional flux for these two gases in the nanopores of the ordered mesoporous silica fibers. The surface diffusion coefficients for the ordered mesoporous silica fibers are about 1 order of magnitude larger than the nonordered mesoporous alumina or silica with similar pore size.

1. Introduction

Mesoporous silica fibers (MSF) prepared under stagnant two-phase acidic conditions[1] exhibit hexagonal pore arrangement typical of MCM-type materials[2] according to powder X-ray diffraction (XRD) measurements. The original report on the preparation of ordered MSF[1] states that the pores align parallel to the fiber axis as suggested for other types of silica-based fibers.[3−5] However, subsequent studies on silica fibers prepared with tetrabutyl orthosilicate (TBOS) revealed a circular inner architecture of the pores according to transmission electron microscopy (TEM) and birefringence investigations.[6,7] The hexagonal array of channels in TEM overviews appears to be perpendicular to the fiber axis on both fiber edges suggesting that the channels have a helical structure with very small pitch angle of the helix. The helical pore orientation was found to be a common structure for the two-phase acidic synthesis of silica fibers based on various types of silica sources.[8]

No study has been reported so far on the measurement of the inner pore microscopic dimensions of the helical channels including the pore length, pitch size, and tortuosity. This could be useful in a number of practical applications such as modulated channel-based nanoreactors and polymer molecular extrusion where channel length affects the yield, conversion, and structure of the product. Representative measurement of the pore length and pitch size seems to be impossible with direct techniques such as TEM due to sensitivity of results to imaging location and sampling conditions. Besides, the fiber thickness would not allow viewing the helical pores across the length direction perpendicular to the fiber axis.

Most studies on the ordered nanoporous materials have focused on the synthesis and microstructure of this group of materials. Equilibrium sorption of gases and vapors on ordered nanoporous silicates such as MCM-41 has also been extensively studied for material characterization or exploring the use of this group of materials as sorbents.[9] However, essentially no studies were reported on gas diffusion in the ordered nanoporous materials. Available investigations on gas transport in these materials are limited to steady-state gas permeance of 3-D pore MCM-48 prepared as supported membranes to study their quality.[10−12] Gas permeance of 1-D ordered mesoporous silica (like MCM-41 and MSF) membranes has not been studied yet because no one was able to orient the pores preferentially normal to the support surface.[13]

Unsteady-state techniques were also used to measure diffusion properties of porous solids of powder and membrane geometries.[14] Transient weight uptake is one example of this approach in which the rate of change in sample weight due to gas adsorption is measured and used to evaluate diffusion properties. To our best knowledge, up to now no one has measured the transient uptake properties for ordered mesoporous materials probably due to the anticipation of fast gas diffusion rate in nanoporous particles. The diffusion time constant (L^2/D) for 5 μm MCM-41 particles (assuming Knudsen diffusion, with $D \sim 10^{-2}$ cm^2/s) could be several orders of magnitude smaller than that for 5 μm zeolite silicalite crystallites (zeolitic diffusion, $D \sim 10^{-8}$ cm^2/s). This makes it difficult to experimentally measure gas diffusion in the ordered mesoporous particles unless the diffusion study involves large gas molecules[15] or much larger ordered mesoporous particles are available.

Gas transport through ordered mesoporous materials is governed by the Knudsen diffusion mechanism with negligible contribution from viscous flow. If the pore surface tends to adsorb the gas molecules, additional flux contribution may come from diffusion of the adsorbed phase on the surface. Surface diffusion contributes significantly to transport in microporous and mesoporous materials and in some cases it accounts for over 50% of the total flow rate.[16] Gas transport mechanisms were identified for various porous mesoporous materials;[14] however, little attention was given to study the significance of the structural order of the pores on the transport mechanisms and their contributions. Such knowledge will be a guide to

* Corresponding author. Phone: (480) 965-7769. Fax: (480) 965-0037. E-mail: jerry.lin@asu.edu.
† University of Cincinnati.
‡ Current address: Chemical and Biomolecular Engineering, Georgia Institute of Technology, Atlanta, GA 30332.
§ Arizona State University.

10.1021/jp0509764 CCC: $30.25
Published on Web 06/24/2005

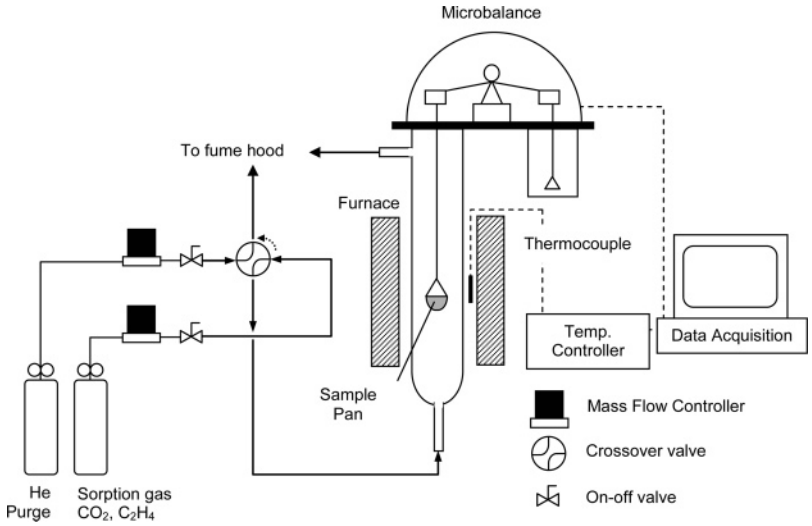

Figure 1. Schematic of the Cahn C-1000 microbalance system apparatus for measurement of gas sorption−diffusion in mesoporous silica fibers.

significant improvement in the design and applications of these materials as catalysts, membranes, and sorbents in unprecedented ways.

This paper reports on transient weight uptake measurements of ordered MSF by the gravimetric method. Such measurements become feasible because of the availability of large ordered mesoporous silica fibers prepared in our laboratory. The uptake data are treated with a suitable diffusion model to study the gas diffusion properties in the ordered structure and its effect on the relative contribution of each diffusion mechanism. For the first time this paper demonstrates the use of the gas diffusivity data to elucidate the inner microstructural dimensions of the one-dimensional ordered mesopores such as the pore length and shape.

2. Experimental Section

Mesoporous silica fibers were prepared by the interfacial approach at acidic and quiescent (no mixing) conditions with tetrabutyl orthosilicate (TBOS) (Aldrich) as the silica source and cetyltrimethylammonium bromide (CTAB) (Aldrich) as the structure directing agent.[17] The morphology was studied with SEM (Hitachi-S4000). Powder X-ray diffraction (XRD) patterns were obtained on Siemens D-50 with use of Cu Kα radiation. XRD spectra were taken between 2θ of 1.5−8 and used to identify the phase structure. Nitrogen adsorption−desorption measurements were performed on Micromeritics Tristar to obtain pore surface area, volume, and size properties.

Sorption experiments were conducted gravimetrically on a Cahn electronic microbalance system (CAHN C-1000),[18] as shown in Figure 1. One arm of the microbalance had an aluminum pan suspended at its end to hold the sample. The pan was attached to the microbalance arm by a light platinum wire (Gauge 36, Fisher Scientific). The pan was maintained at the desired temperature with an Omega CN 76000 temperature controller connected to a tubular furnace mounted on the outside of a 2 in. i.d. Pyrex balance tube. The furnace was mounted so that the sample pan was approximately at its center. The temperature was measured by a thermocouple (K-type Omega KMTSS-032G-12). The gas delivery system consisted of a helium purge gas and several sorption gases of various molecular weights (CO_2, C_2H_4, N_2, H_2, O_2, and CH_4). The purge and sorption gases were alternatively delivered to the system by switching a crossover valve (Swagelock). The transient and equilibrium weight changes were recorded with use of a computer-aided data acquisition system.

In experiments, a 200−300 mg sample of MSF was loaded to the lightweight (200 mg) aluminum pan and degassed at 120 °C for a few hours under helium purge flow at 100 mL/min. After the sample weight became constant, the temperature was cooled to the desired sorption temperature (room temperature). Then the adsorption process was started by switching from the purge gas to the sorption gas at 100 mL/min, using the crossover valve. After the adsorption process reached equilibrium, gas desorption was conducted at the same temperature by switching back to purge gas at 100 mL/min. The 100 mL/min flow rate was found optimum where systematic problems of gas dispersion (caused by switching between gases) and weight instability (taking place at high flow rates) were minimized. Data were deduced to obtain uptake (mg gas adsorbed/g adsorbent or mmol/g) and fractional uptake rate (uptake/equilibrium uptake) curves. Gas adsorption isotherms were measured at room temperature by adsorption of the gas in helium, with the gas partial pressures varied between 0 and 1 atm.

3. Results and Discussion

3.1. Characteristics of Mesoporous Silica Fibers. The XRD pattern of MSF product exhibits three reflection peaks indexed as 100, 110, and 200 typical of hexagonal pore arrangement. Nitrogen sorption isotherms on silica fibers are shown in Figure 2. They exhibit type-IV response typical to mesoporous materials with well-aligned channels. The first step in the adsorption isotherm is associated with monolayer coverage of nitrogen molecules on the inner surface and the second step is due to capillary condensation within the cylindrical pores. The adsorption and desorption isotherms almost coincide with no hysteresis, which is a characteristic of mesoporous silica materials with pore diameters less than 3.8 nm.[19] A narrow pore size distribution, inset of Figure 2, with a mean BJH diameter of 2.74 nm was obtained from the desorption branch. This value is similar to that obtained from the adsorption branch indicative of uniform cylindrical pore shapes. The fibers have a BET surface area of 799 m^2/g and a pore volume of 0.62 cm^3/g. From the pore volume and silica density (2.15 g/mL) the porosity was calculated as 0.571. The fibers are 15 μm in diameter and have an average length of 196 μm, as measured by SEM micrographs.[17]

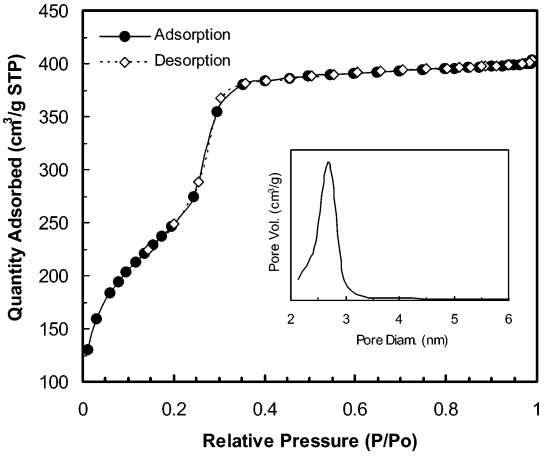

Figure 2. Nitrogen adsorption−desorption isotherms for mesoporous silica fibers. Inset is the pore size distribution obtained from the desorption branch by the BJH method.

3.2. Gas Uptake on Silica Fibers. Kinetic gas uptake measurements on MSF were performed with gases of various molecular weights. Due to the nature of physical adsorption of gases on MSF, no adsorption was observed at temperatures over 60 °C for all gases. Therefore, all experiments were performed at room temperature to obtain uptake values with reasonable accuracy. Lower temperatures could not be applied due to limited temperature control of our equipment with a lowest achievable value of room temperature. Experiments showed that sorption uptakes for N_2, H_2, O_2, and CH_4 on MSF were too small (compared with the perturbation of the microbalance with respect to a switch in gas flow) to allow accurate determination of diffusivity. CO_2 and C_2H_4 exhibited sufficiently high sorption uptakes for accurate measurements of diffusivity. Therefore sorption experiments were focused on these two gases.

Absolute and fractional rate of weight uptake of CO_2 and C_2H_4 and on MSF at 28 °C and 1 atm are shown in Figure 3, where the fractional uptake is the ratio of the uptake at time t (M_t) to the equilibrium uptake (M_∞). Uptake capacities of CO_2 and C_2H_4 are respectively 0.68 and 0.78 mmol/g, which are equivalent to 29.92 and 21.84 mg/g. Gas uptake under these conditions is far below the monolayer coverage of MSF. The percentage of monolayer coverage is estimated as 4.6% and 7.0% for CO_2 and C_2H_4, using the equation $X_{\text{monolayer}} = q A_o N_A / S_A$, where q (mol/g) is the uptake capacity, S_A is the BET surface area (799 m^2/g), A_o is the sorbate cross sectional area estimated from the molecular kinetic diameter assuming a spherical shape (9 Å^2 for CO_2 and 12 Å^2 for C_2H_4), and N_A is Avogadro's number (6.02×10^{23} molecule/mol).

Fractional uptake of C_2H_4 is faster than that of CO_2 indicating a slightly larger diffusion coefficient. Kinetic sorption curves of these gases in MSF consist of a steep uptake step up to 90% in less than 3 min followed by a slowly increasing uptake achieving M_∞ plateau within 10 min. Contrary to the anticipated fast gas diffusion rate in the ordered mesoporous materials (governed by Knudsen-type diffusion), the response time in MSF was slow enough to be experimentally measured with acceptable accuracy. This is due to high resistance to gas diffusion as a result of the long straight pores aligned within the fibers.

Transient weight uptake data can be utilized to investigate the gas diffusion properties and to elucidate the fiber microstructural properties. The fibers contain a huge number of one-dimensional nanosized cylindrical pores aligning helically around the fiber axis.[6,7] Diffusion of gases in the pores can be considered as one-dimensional bounded by the two sides of the fiber. Such a diffusion process is approximately described by the plain sheet model of unidimensional diffusion[20] shown in eq 1, where D_{eff} is the effective diffusion coefficient and L is the fiber length.

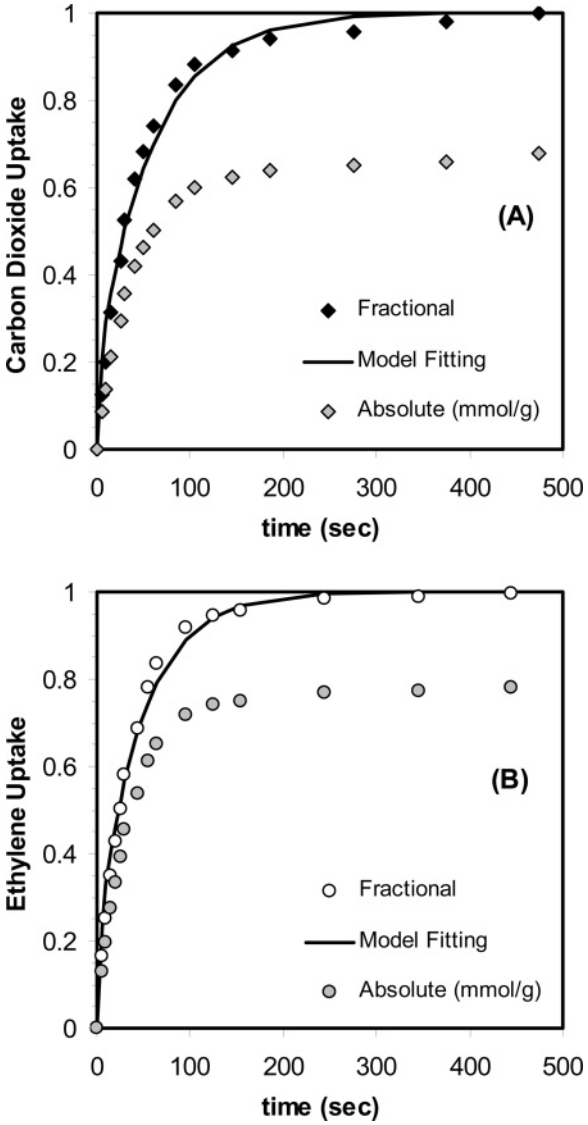

Figure 3. Absolute and fractional uptake of CO_2 (A) and C_2H_4 (B) on mesoporous silica fibers (solid curve is the model fitting on experimental data).

$$\frac{M_t}{M_\infty} = 1 - \sum_{n=0}^{\infty}\left[\frac{8}{(2n+1)^2\pi^2}\exp\left(\frac{-(2n+1)^2\pi^2}{4}\frac{D_{\text{eff}}}{L^2}t\right)\right] \quad (1)$$

The time constant (D_{eff}/L^2) was obtained by regression of the fractional uptake data with eq 1 by Mathematica, using the least-squared method. The best-fit uptake curves for CO_2 and C_2H_4 calculated from eq 1 are plotted in Figure 3 (solid line) with the experimental data. D_{eff} can be subsequently calculated and used to analyze the diffusion properties for the ordered mesoporous fibers. From Figure 3, the best fit of the diffusion model to experimental data was obtained with D_{eff}/L^2 values of 6.68×10^{-3} s^{-1} for CO_2 and 8.54×10^{-3} s^{-1} for C_2H_4 from which D_{eff} can be calculated respectively as 2.57×10^{-6} and 3.28×10^{-6} cm^2/s (where L is the average fiber length of 196 μm).[17]

3.3. Evaluation of Transport Diffusivities. Single gas diffusion through porous materials can be generally described by Ficks law $J_i = D_{eff}\, dC_i/dl$, where J_i is the molar flux, dC_i/dl is the concentration gradient, and D_{eff} is the effective diffusivity of the component i. D_{eff} represents a combination of all mechanisms of transport, which can be in the gaseous phase of the pore by viscous or Knudsen diffusion or on the pore surface by surface diffusion. Results of gas uptake show that MSF has a tendency to physically adsorb CO_2 and C_2H_4 molecules with low concentrations. The molecules in the adsorbed phase can exhibit mobility on the pore surface by hopping between the adsorption sites under the effect of surface concentration gradient. This mobility can considerably increase the net flux by an additional surface diffusion term. C_2H_4 is expected to have more surface diffusion flow than CO_2 because it has a higher uptake capacity on MSF. The viscous flow in the 3 nm pores of MSF can be neglected; therefore, the gas phase diffusion in MSF pores is mainly caused by the Knudsen mechanism. The ratio of effective pure gas diffusivities can be used to roughly identify the presence of an additional surface diffusion contribution. The ideal diffusivity ratio of C_2H_4 to CO_2 based on the Knudsen flow is equal to the squared root of the molecular weight of CO_2 to C_2H_4 [$=(44/28)^{0.5} = 1.25$]. The real diffusivity ratio of C_2H_4 to CO_2 is 1.39, which is higher than the Knudsen-based ratio. This confirms that CO_2 and C_2H_4 diffuse by a combined Knudsen and surface flow in the ordered pores of MSF. The surface contribution of nonadsorbing gases will be negligible. Since both mechanisms take place in parallel, the total effective diffusion can be represented as a linear combination of the two mechanisms as expressed in eq 2[14] under ideal gas phase and equilibrium adsorption−desorption isotherm conditions. $D_{K,eff}$ and $D_{S,eff}$ are the effective Knudsen and surface diffusivities, respectively, ϵ is the porosity of MSF (0.571), and K is the dimensionless adsorption equilibrium constant.

$$D_{eff} = D_{K,eff} + \frac{1-\epsilon}{\epsilon} K D_{S,eff} \tag{2}$$

Direct calculation of $D_{K,eff}$ and $D_{S,eff}$ for each gas from one uptake curve at room temperature is impossible. One strategy is to measure the diffusion of a nonadsorbing calibration gas for which the diffusion is governed by Knudsen mechanism (D_K) then to measure the combined surface and Knudsen diffusion for a desired gas. The Knudsen contribution of the gas can be found with the following relationship: $D_{Ki} = D_{K,nonads}(M_{nonads}/M_i)^{0.5}$, then the surface contribution can be evaluated from the linear combination of diffusion coefficients with eq 2.[21] Another way is to run the uptake experiment at high temperature (e.g., 200 °C) and obtain D_{eff}, which will be equivalent to $D_{K,eff}$ because the contribution of surface diffusion becomes negligible (with very small K value) at high temperatures. Both cases, however, could not be performed on MSF because of the low uptake capacity of the nonadsorbing gases (H_2 and N_2) and the negligible sorption uptakes at high temperature.

In this work, an alternative analytical approach was used to obtain the diffusion coefficients of gases in the ordered MSF. Knudsen and surface diffusion contributions were predicted utilizing a simple model based on theoretical diffusion relations, experimentally obtained time constant (D_{eff}/L^2) of eq 1, and adsorption equilibrium constant (K) of adsorbing gases at room temperature. Knudsen[14] and surface[22] diffusivities can be expressed as:

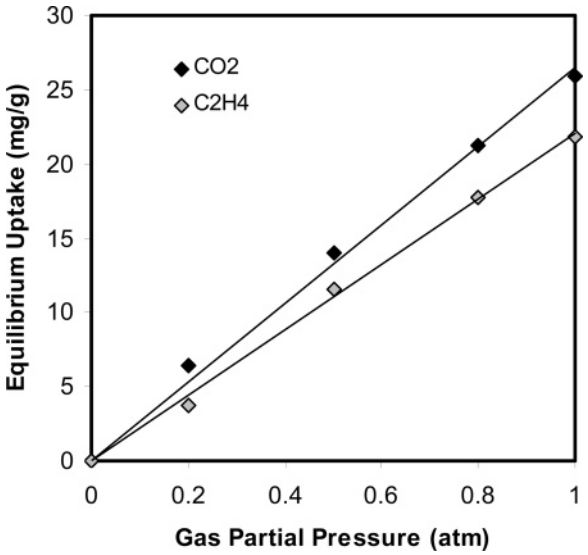

Figure 4. Equilibrium adsorption isotherms of CO_2 and C_2H_4 on silica fibers at 28 °C and partial pressure 0−1 atm.

$$D_{K,eff} = \frac{\epsilon}{\kappa} d_p \sqrt{\frac{8RT}{9\pi M}} \tag{3}$$

$$D_{S,eff} = \frac{BT\sqrt{T}\exp(-E/RT)}{\sqrt{M}} \tag{4}$$

where κ, ϵ, and d_p are respectively the tortuosity factor, porosity, and pore diameter of MSF. T and M are the temperature and molecular weight of diffusing gas. E is the surface diffusion activation energy and B is constant. Both diffusivities have similar dependency on the square root of the gas molecular weight. It should be pointed out that the tortuosity factor (κ) and the tortuosity (τ) are different.[23] Tortuosity factor (κ) is the square of tortusosity (τ), which is defined as the ratio of diffusion length to macroscopic length, i.e., $\kappa = \tau^2 =$ (diffusion length/macroscopic length).[2] Substitution of eqs 3 and 4 in eq 2 and simplification give the following form:

$$\frac{D_{eff}}{L^2}\sqrt{M} = \alpha + \beta K \tag{5}$$

with the temperature constants α and β given by:

$$\alpha = \frac{\epsilon}{\kappa}\frac{d_p}{L^2}\sqrt{\frac{8RT}{9\pi}} \tag{6}$$

$$\beta = \frac{(1-\epsilon)}{\epsilon}\frac{BT\sqrt{T}\exp(-E/RT)}{L^2} \tag{7}$$

Dealing with eq 5 is much easier than with eq 2. D_K and D_S vary with the gas used and the experimental conditions. Obtaining these values for two gases by using eq 2 is impossible because there will be two equations ($y_i = D_{Ki} + D_{Si}x_i$, where $y_i = D_{eff,i}/L^2$ and $x_i = K_i(1-\epsilon)/\epsilon$ for each gas) and four unknowns (D_{K1}, D_{S1}, D_{K2}, and D_{S2}). Equation 5 is an extension of eq 2 but the constants, α and β, will be the same for any gas used. Therefore, these constants can be evaluated easily for two gases by using two equations ($y_i = \alpha + \beta x_i$, where $y_i = D_{eff,i}(M_i)^{0.5}/L^2$ and $x_i = K_i$ for each gas) and two unknowns

TABLE 1: Experimental Parameters of Diffusing Gases in Mesoporous Silica Fibers (at Room Temperature)

gas	M (mol/g)	K (dimensionless)	D_{eff}/L^2 (s^{-1})	$(D_{eff}/L^2)(M)^{0.5}$
CO_2	44	31.94	6.68×10^{-3}	0.044
C_2H_4	28	41.66	8.54×10^{-3}	0.045

TABLE 2: Knudsen and Surface Diffusivities and Contribution to Net Gas Diffusion in MSF

gas	D_{eff} (cm^2/s)	$D_{K,eff}$ (cm^2/s) (%)	$(1-\epsilon_p/\epsilon_p)KD_{S,eff}$ (cm^2/s) (%)	$D_{S,eff}$ (cm^2/s)
CO_2	2.57×10^{-6}	2.41×10^{-6} (94%)	1.61×10^{-7} (6%)	6.71×10^{-9}
C_2H_4	3.28×10^{-6}	3.02×10^{-6} (92%)	2.63×10^{-7} (8%)	8.41×10^{-9}

(α and β) and then be used to evaluate D_K and D_S with eqs 3 and 6 and eqs 4 and 7, respectively. Moreover, by using eq 6, the tortuosity factor (κ) can be evaluated and used to analyze the pore structure of the ordered silica fibers such as pore length and orientation.

Figure 4 shows the adsorption isotherms of CO_2 and C_2H_4 on MSF measured at room temperature and 0 to 1 atm partial pressures. Gas adsorption capacity of MSF at room temperature is close to 25 mg/g, which is almost 5−7% of the monolayer capacity based on its surface area. This value is consistent with the gas adsorption capacity of the unmodified ordered MCM-41 silica.[24] C_2H_4 has a higher molar adsorption capacity than CO_2 and this implies a higher surface flow contribution. The isotherms are reasonably linear with low uptake capacities below the monolayer surface coverage so K can be evaluated directly from the slope. Dimensionless equilibrium constant K (defined as moles adsorbed per unit solid volume/moles per unit volume in the gas phase) can be obtained from the slope of the isotherm shown in Figure 4 by using eq 8:

$$K = \text{slope (g/g·atm)} \times \frac{RT\rho_{solid}}{M} \tag{8}$$

where R is the ideal gas constant (82.1 atm·mL/mol·K), T is temperature (300 K), ρ_{solid} is the silica density (2.15 g/mL), and M is the gas molecular weight (g/mol). Adsorption isotherms have slopes of 26.54×10^{-3} and 22.03×10^{-3} g/g·atm respectively for CO_2 and C_2H_4 from which K values were calculated as 31.94 and 41.66.

Table 1 summarizes the experimental values that were used to estimate the constant parameters of eq 5. A plot of $(D_{eff}/L^2)(M)^{0.5}$ versus K gives values respectively of 4.15×10^{-2} and 8.70×10^{-5} $(g/mol)^{0.5}/s$ for constants α and β. The intercept (α) is a temperature constant value that is related to the Knudsen diffusivity while the slope (β) is related to the surface diffusivity. The effective Knudsen diffusivity ($D_{K,eff}$) was calculated from eqs 3 and 6 then the surface contribution ($KD_{S,eff}$) was evaluated by subtracting the Knudsen contribution from the total effective diffusion coefficient with eq 2. Diffusivities and contribution of diffusion mechanisms are summarized in Table 2.

According to the gas uptake results and data fitting with the plane sheet model, the overall effective diffusivity of gases under study is in the range of $(2.5-3.3) \times 10^{-6}$ cm^2/s. Knudsen diffusion is the major mechanism of gas-phase diffusion in the ordered fibers. It contributes to almost 90% of the transport in the straight pores, while the remaining is contributed by the surface mechanism. The slight difference in the diffusion contributions observed by CO_2 and C_2H_4 gases is accounted for by the difference in their diffusion and adsorption behaviors. According to eqs 3 and 4, C_2H_4 will have higher Knudsen and surface diffusivities than CO_2 because it has a smaller molecular weight. Moreover, it exhibited a higher molar adsorption capacity and adsorption equilibrium constant (K) and therefore had a higher diffusivity than CO_2. A nonadsorbing gas such as N_2 or He, on the other hand, will have a negligible surface diffusion contribution and the net diffusion will be solely governed by the Knudsen mechanism. It is worth mentioning, however, that diffusion properties of such gases could not be evaluated by the gravimetric approach as a result of their negligible weight uptakes.

TABLE 3: Effective and Real Gas Diffusion Coefficients in MSF

	D_K (cm^2/s)		D_S (cm^2/s)	
gas	effective	real	effective	real
CO_2	2.41×10^{-6}	3.47×10^{-3}	6.71×10^{-9}	5.52×10^{-6}
C_2H_4	3.02×10^{-6}	4.35×10^{-3}	8.41×10^{-9}	6.92×10^{-6}

Sholl and co-workers reported exceptionally high transport diffusivities of light gases in microporous single-walled carbon nanotubes (SWCN) up to 10 cm^2/s using atomistic simulation.[25] These values are at least 2 orders of magnitude larger than those exhibited by silicalite and ZSM-12 microporous zeolites of similar pore sizes. The fast diffusivities were attributed to the surface smoothness that can strongly control the solid−sorbate interaction potentials. Given the similarity in pore dimensionality (1D), pore length, and pore curvature features of the MSF pores and the carbon nanotubes, we can assume that the slight 10% contribution of surface flow in MSF can be attributed to the smoothness of the pore surface.

It should be noted that the effective surface diffusivity measured in this study includes the effects of surface roughness or surface groups, e.g., silanol, which do not influence the effective Knudsen diffusivity. Variation of the surface roughness and surface groups will affect the adsorption properties, overall effective diffusivity, and effective surface diffusivity, but not the effective Knudsen diffusivity, which will be used to calculate pore tortuosity and pore length as will be shown next.

The effective diffusivities given in Table 2 can be related to the real diffusivity expressed in terms of diffusivity in a straight cylindrical pore of equivalent diameter by:[26]

$$D_{eff} = \frac{\epsilon}{\kappa_g} D_{K,real} + \frac{(1-\epsilon)K}{\epsilon} \frac{D_{S,real}}{\kappa_s} \tag{9}$$

From eq 9, $D_{K,eff} = (\epsilon/\kappa_g)D_{K,real}$ and $D_{S,eff} = (1/\kappa_s)D_{S,real}$, where κ_g and κ_s are the gas (void) and surface tortuosity factors, respectively. Tortuosity is a lumped structural factor defined as the length of the equivalent capillary required to describe the effective diffusivity in the void or surface phases. For the case of MSF, κ_g was estimated from eq 6 as 823, which reflects a highly tortuous structure. The value of κ_s could not be evaluated with eq 7 because the constants B and E are unknown. Besides, κ_g and κ_s are not equivalent because the distance traveled by molecules in the pore is different from that on the surface especially with systems of irregular pore structure. Given that MSF has a regular cylindrical pore structure with uniform pore size distribution in the low limit of the mesoporous size (2.74 nm), the difference in diffusion path between the gas phase and the surface is not significant. Therefore, we can reasonably assume that κ_g and κ_s of MSF are equal.

Real Knudsen and surface diffusivities were accordingly calculated by using eq 9 and summarized in Table 3. Real Knudsen diffusivity of ordered MSF is in the range of $\sim 10^{-3}$ cm^2/s, which is consistent with values of mesoporous

TABLE 4: Real Surface Diffusivities of CO_2 in Ordered Mesoporous Silica Fibers versus Other Nonordered Porous Solids

sorbent (pore size)	temp (°C)	measurement method	surface flow contribution (%)	D_S (cm^2/s)	ref
MSF (2.7 nm)	28	unsteady state gravimetric uptake	6	5.52×10^{-6}	this work
γ-alumina (2.7 nm)	20	steady state Wicke−Kallenbach	30	$2.0-5.0 \times 10^{-5}$	Kiezer et al.[30]
Boehmite (Bimodal)[a]	25	steady state Wicke−Kallenbach	54	9.2×10^{-5}	Rivarola and Smith[21]
Vycor Glass (4.6 nm)	−50	steady state permeability	53	6.0×10^{-5}	Gilliland et al.[31]

[a] Bimodal pore size distribution of 4 and 60 nm.

materials. For most conventional mesoporous materials, the effective diffusivity is typically 1 order of magnitude smaller than the real diffusivity, given a typical porosity and tortuosity values of 0.3 and 3, respectively.[14] In case of MSF, the porosity is similar to that of other mesoporous materials, but the large tortuosity factor (823) is the main reason for the significant reduction in effective transport properties by 3 orders of magnitude.

Although gas diffusion in mesoporous materials has been extensively studied over the past decades, only a few papers have focused on CO_2 and C_2H_4 diffusion at room-temperature conditions. Table 4 gives a summary of the major CO_2 real surface diffusivities reported on common nonordered mesoporous alumina and Vycor glass in comparison with results on ordered MSF. In contrast to the hexagonally ordered cylindrical pores of MSF, γ-alumina has irregular slit shaped pores,[27] while Vycor glass has a 3-D irregular pore structure made by random packing of spheroidal glass particles.[28] The diffusivity data for those nonordered mesoporous materials were measured on the membranes of these materials by a more reliable steady-state permeation method.

To have a rational comparison, diffusion coefficients must be obtained or at least treated on the same experimental basis. Reyes and co-workers[29] discussed the discrepancies in diffusion parameters obtained by steady- and unsteady-state techniques in terms of the adsorption capacity factor (ACF) $= 1 + KS_v$, where K is the adsorption equilibrium constant (at sufficiently low concentration) and S_v is the average surface-to-volume ratio (S_v = 4/pore diameter for cylindrical pores). The effective diffusion coefficient obtained in an unsteady-state measurement differs from that obtained in a steady-state experiment by the ACF factor (i.e., $D_{unstaedy} = D_{steady}$/ACF). For a nonadsorbing gas, the ACF value will reduce to unity (since $K = 0$) and give similar steady and unsteady diffusivities. The ACF value for CO_2 diffusion MSF was calculated as ~30. By using the equation $D_{unstaedy} = D_{steady}$/ACF, the effective diffusivity of CO_2 in MSF will be 30-fold higher if measured by a steady-state approach. Thus, the surface diffusivity in the ordered MSF is about 1 order of magnitude higher than diffusion in nonordered mesoporous materials. This suggests that the ordered structure can significantly enhance the diffusion properties possibly due to lower transport resistances associated with the regular packing of the pores.

3.4. Fiber Internal Microstructure. The gas-phase tortuosity factor (κ_g) of MSF was calculated in the previous section from eq 6 as 823 and was assumed to be equal to the surface tortuosity (κ_s). This value is very high compared to typical tortuosities of porous solids.[14] The tortuosity factor can be used to provide more information about the internal microstructure of the porous material. It is generally given by the ratio $(l_p/L)^2$,[23] where l_p is the length of tortuous diffusion path and L is the mean thickness of the diffusion path. This ratio defines the commonly used tortuosity (τ) value. MSF has an internal structure composed of cylindrical pores that align helically across the fiber axis as suggested in the literature from TEM images. In this case, l_p will be the length of the helical pores inside the fiber and L is the average length of fibers (196 μm). From $\kappa = 823$, the ratio l_p/L ($=\tau$) was found to be 29. This means that the pores are 29 times longer than the fiber macroscopic length. From this ratio we can imagine that a 196 μm long fiber will contain 6 mm long pores. Given that the pores are cylindrical and nonconnected as revealed by TEM images, and are much longer than the fiber length, the only possible orientation of these pores is to whirl helically across the fiber as schematically illustrated in Figure 5.

Although the helical orientation was previously suggested by other investigators by a direct image method, this study confirms the helical pore structure and provides information on the microscopic dimensions of these pores. The degree of orientation or pitch length (z) can be estimated from the fiber diameter (d_f =15 μm), fiber length (L), and pore length (l_p) by using the equation $l_p = \pi d_f L/z$ (where $l_p/L = 29$). This corresponds to a pitch value of 1.6 μm. The degree of pore orientation and pitch measurement is illustrated in Figure 5. Such measurements are very hard if not impossible by direct techniques such as TEM images.

It should be noticed that these microscopic dimensions, i.e., pore length and pitch size, represent the average values. In fact, the pores have a distribution in their length. By imagining the hexagonal packing of the cylindrical pores, the formation of the internal structure by cylindrical rod micelles proceeds as

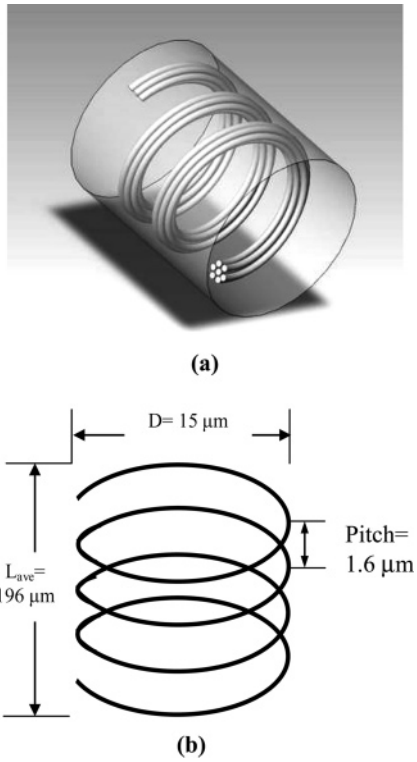

Figure 5. Schematic representation of the internal pore structure of silica fibers: (a) helical pore orientation of the hexagonally arranged pores and (b) approximate internal pore dimensions (length, diameter, and pitch) with a tortusosity factor of 29.

follows: the first micelle starts to whirl around an imaginary vertical axis, then additional rod micelles whirl helically around each other with hexagonal packing to grow the fiber in length and diameter. This process continues until it ends up with the final observed macroscopic dimensions of the fiber. The outer pore will therefore be longer than the internal pores. The pitch on the other hand is not expected to change significantly due to the long-range order of the hexagonal packing of the pores. The pore microstructure and dimensions of MSF obtained in this study provide new fundamental information on the formation process. Technically, such information together with the diffusion properties have a significant impact on the design and application of this group of ordered materials in membrane reactors, catalysis, and separation to name a few. In reactor application, pore length and diffusion properties can be used to understand the production process and to improve product yield and quality.

4. Conclusions

N_2, H_2, O_2, and CH_4 exhibit negligible adsorption on ordered mesoporous silica fibers at room temperature. Adsorption of CO_2 and C_2H_4 on the ordered mesoporous silica fibers (MSF) at room temperature follows a linear adsorption isotherm with sorption capacities of close to 25 mg/g at 1 atm partial pressure. The plain sheet diffusion model was used to fit the weight uptake data to obtain the overall effective diffusivities in MSF. The ratio of the effective diffusivities of the two gases was different from the Knudsen-based ratio indicating the presence of a surface diffusion contribution to the net flow. A simple model was derived and utilized to separate the contribution of each mechanism, using the data obtained by the transient uptake measurements. The surface diffusion mechanism contributes to ~10% of the net flow. The surface diffusivity in the ordered mesoporous silica is about 1 order of magnitude larger than that of the nonordered mesoporous materials. The pore diffusivity data were used to calculate the actual length of the nanopores in the silica fibers, and the results reveal a structure of the fibers with nanopores aligning helically across the fiber axis, with the spiral diameter of about 15 μm and a pitch value of 1.6 μm, confirming the literature investigations based on TEM images.

Acknowledgment is made to the donors of the Petroleum Research Fund, administered by the American Chemical Society, for support of this work.

References and Notes

(1) Huo, Q.; Zhao, D.; Feng, J.; Weston, K.; Buratto, S. K.; Stucky, G. D.; Schacht, S.; Schuth, F. *Adv. Mater.* **1997**, *99*, 74.

(2) Beck, J. S.; Vartuli, J. C.; Roth, W. J.; Leonowizc, M. E.; Kresge, C. T.; Shmitt, K. D.; Chu, C. T.; Olson, D. H.; Shepard, E. W.; McCullen, S. B.; Higgins, J. B.; Schlenker, J. L. *J. Am. Chem. Soc.* **1992**, *114*, 10834.

(3) Yang, P.; Zhao, D.; Chmelka, B. F.; Stucky, G. D. *Chem. Mater.* **1998**, *10*, 2033.

(4) Han, Y. J.; Kim, J. M.; Stucky, G. D. *Chem. Mater.* **2000**, *12*, 2068.

(5) Miyata, H.; Kurod, K. *Adv. Mater.* **2001**, *13*, 558.

(6) Marlow, F.; Slpliethof, B.; Tesche, B.; Zhao, D. *Adv. Mater.* **2000**, *12*, 961.

(7) Marlow, F.; Kleitz, F. *Microporous Mesoporous Mater.* **2001**, *44*−*45*, 671.

(8) Kleitz, F.; Marlow, F.; Stucky, G. D.; Schuth, F. *Chem. Mater.* **2001**, *13*, 3587.

(9) Selvam, P.; Bhatia, S. K.; Sonwane, C. G. *Ind. Eng. Chem. Res.* **2001**, *40*, 3237.

(10) Nishiyama, N.; Park, D. H.; Koide, A.; Egashira, Y.; Ueyama, K. *J. Membr. Sci.* **2001**, *182*, 235.

(11) McCool, B. A.; Hill, N.; DiCarlo, J.; DeSisto, W. J. *J. Membr. Sci.* **2003**, *218*, 55.

(12) Xomeritakis, G.; Naik, S.; Braunbarth, C. M.; Cornelius, C. J.; Pardey, R.; Brinker, C. J. *J. Membr. Sci.* **2003**, *215*, 225.

(13) Alsyouri, H. M.; Langheinrich, C.; Lin, Y. S.; Ye, Z.; Zhu, S. *Langmuir* **2003**, *19*, 7307.

(14) Karger, A.; Ruthven, D. M. *Diffusion in Zeolites and other Microporous Solids*; J. Wiley & Sons. Inc.: New York, 1992; Chapter 11, p 342.

(15) Berenguer-Murcia, A.; Fletcher, A. J.; Garcia-Martinez, J.; Cazorla-Amoros, D.; Linares-Solano, A.; Thomas, K. M. *J. Phys. Chem. B.* **2003**, *107*, 1012.

(16) Choi, J. G.; Do, D. D.; Do, H. D. *Ind. Eng. Chem. Res.* **2001**, *40*, 4005.

(17) Alsyouri, H. M.; Lin, Y. S. *Chem. Mater.* **2003**, *15*, 2033.

(18) Chandak, M. V.; Lin, Y. S.; Ji, W.; Higgins, R. J. *J. Membr. Sci.* 1997, *133*, 231.

(19) Inoue, S.; Hanzawa, Y.; Kaneko, K. *Langmuir* **1998**, *14*, 3079.

(20) Crank, J. *The Mathematics of Diffusion*; Clarsndon Press: Oxford, UK, 1975; Chapter 4, p 44.

(21) Rivarola, J. B.; Smith, J. M. *Ind. Eng. Chem. Fundam.* **1964**, *3*, 308.

(22) Hwang, S. T.; Kammermeyer, K. *Can. J. Chem. Eng.* **1966**, 82.

(23) Epstein, N. *Chem. Eng. Sci.* **1989**, *44*, 777.

(24) Xu, X. C.; Song, C. S.; Andresen, J. M.; Miller, B. G.; Scaroni, A. W. *Microporous Mesoporous Mater.* **2003**, *1*−*2*, 29.

(25) Skoulidas, A.; Ackerman, D.; Johnson, J. K.; Sholl, D. *Phys. Rev. Lett.* **2002**, *899*, 185901.

(26) Zalc, J. M.; Reyes, S. C.; Iglesia, E. *Chem. Eng. Sci.* **2003**, *58*, 4605.

(27) Lin, Y. S. *J. Membr. Sci.* **1993**, *9*, 55.

(28) Levitz, P.; Ehret, G.; Sinha, S. K.; Drake, J. M. *J. Chem. Phys.* **1991**, *95*, 6151.

(29) Reyes, S. C.; Sinfelt, J. H.; DeMartin, G. J. *J. Phys. Chem. B* **2000**, *104*, 5750.

(30) Keizer, K.; Ulhorn, R. J. R.; Van Vuren, R. J.; Burggraaf, A. J. *J. Membr. Sci.* **1988**, *39*, 285.

(31) Gilliland, E. R.; Baddour, R. F.; Perkinson, G. P.; Sladek, K. J. *Ind. Eng. Chem. Fundam.* **1974**, *13*, 95.